Ground Penetrating Radar Applied to Monumental Stone Conservation: Application to the Rock Necropolis of San Vítor de Barxacova in NW Spain

Mercedes Solla[1] · Gonzalo Buceta-Bruneti[2] · Ahmed Elseicy[1] · Breogán Nieto-Muñiz[3]

Abstract

This paper deals with the application of the Ground Penetrating Radar (GPR) method in the assessment of stone monuments. Compilation of published works and a discussion of their main findings are first addressed. Next, to show the potential of the method, a case study is presented aiming to assess the state of conservation of the rock necropolis of San Vítor de Barxacova (Ourense, Spain) consisting of 56 anthropomorphic graves carved into the natural rock. Fieldwork was carried out using a GPR system equipped with a 2.3 GHz central frequency antenna. The main goal of this study is to provide an effective approach for the detection and localization of internal damages such as fractures and voids. New amplitude-based 2D and 3D imaging strategies are presented aiming to improve damage detection. A new approach was also developed to digitize the extracted information into a point cloud format, thus improving the possibilities for 3D visualization with the surrounding environment. Although a total of 39 graves were surveyed, only 13 graves are included in this paper due to their singularity and relevant results. The potential of using GPR tests for the assessment of the conservation state of monumental stone structures is also discussed.

Article Highlights

- A case study is presented aiming to assess the state of conservation of a rock necropolis (cemetery) in Spain
- New amplitude-based imaging strategies allowed us to detect inner voids and fractures
- A new approach was developed to digitize the extracted information into a point cloud format

✉ Mercedes Solla
   merchisolla@uvigo.es

Extended author information available on the last page of the article

1 Introduction

Cultural heritage is delicate and, once lost, it is unrecoverable and, as such, it should be protected. The protection of built cultural heritage includes historical buildings and monuments, statues, frescoes and mosaics, etc. The common responsibility to safeguard their authenticity for future generations is recognized and, therefore, the diagnosis and conservation of such ancient structures must be particularly cautious with the preservation of their singular and historical character. Consequently, non-destructive testing (NDT) techniques play an important role as non-invasive investigation for preventive damage detection and heritage preservation. Among these, Ground Penetrating Radar (GPR) is widely recognized as one of the most powerful and versatile NDT methods that have been commonly employed for subsurface high-resolution imaging in many archeological and cultural heritage applications (Goodman and Piro 2013), as well as imaging fractures in geological applications (Grasmueck et al. 2005). Nevertheless, only a few published works deal with the GPR application to monumental stone conservation.

GPR is a geophysical method that uses low- and high-frequencies (from 10 to 6 GHz) for the analysis of the propagation capacity of electromagnetic waves through media with different dielectric constants. High-frequency antennas give better resolution, while low-frequency antennas provide more range of penetration. A transmitting antenna emits an electromagnetic signal into the ground, which is partly reflected at the interface between two different media with sufficient dielectric contrast and partly transmitted into deeper layers. Then, the reflections produced are recorded from the receiving antenna. The strength (amplitude) of the reflected fields is proportional to the change in the magnitude of the dielectric constant. As the antenna is moved along the ground surface, a two-dimensional image (known as a radargram or B-scan) is obtained, which is an XZ graphic representation of the detected reflections. The x-axis represents the antenna displacement along the survey line, and the z-axis represents the two-way travel time of the pulse emitted and received. If the time required to propagate to a reflector and back is measured, and the velocity of the signal propagation in the medium is known, the depth of the reflector can therefore be determined. A deep theoretical background can be found in Annan (2003).

This paper consists of a compilation of the published works dealing with the application of the GPR method to the evaluation of monumental stone (e.g., the presence of cracking, fractures, and moisture in building façades or stonework). For this review, historical buildings, monuments, and statues were considered. In addition, a case study is included to show the potential of the GPR method to detect internal damages in granite stones. Particularly, a GPR investigation in the unique site of the rock necropolis of San Vítor de Barxacova (NW Spain) is presented, which aimed to evaluate the state of conservation of several anthropomorphic graves in the complex. Moreover, different amplitude-based imaging and visualization strategies are tested herein in order to improve damage interpretation and a better understanding of the granite deterioration.

1.1 The Necropolis of San Vítor de Barxacova

The necropolis of San Vítor de Barxacova is located in San Lourenzo de Barxacova, in the municipality of Parada de Sil (Ourense, northwest of Spain) (Fig. 1a). It is placed on a rocky outcrop in the middle of a steep hillside on the west bank of the Mao River. The excavations at the site were carried out between 2010 and 2013. Although only three graves
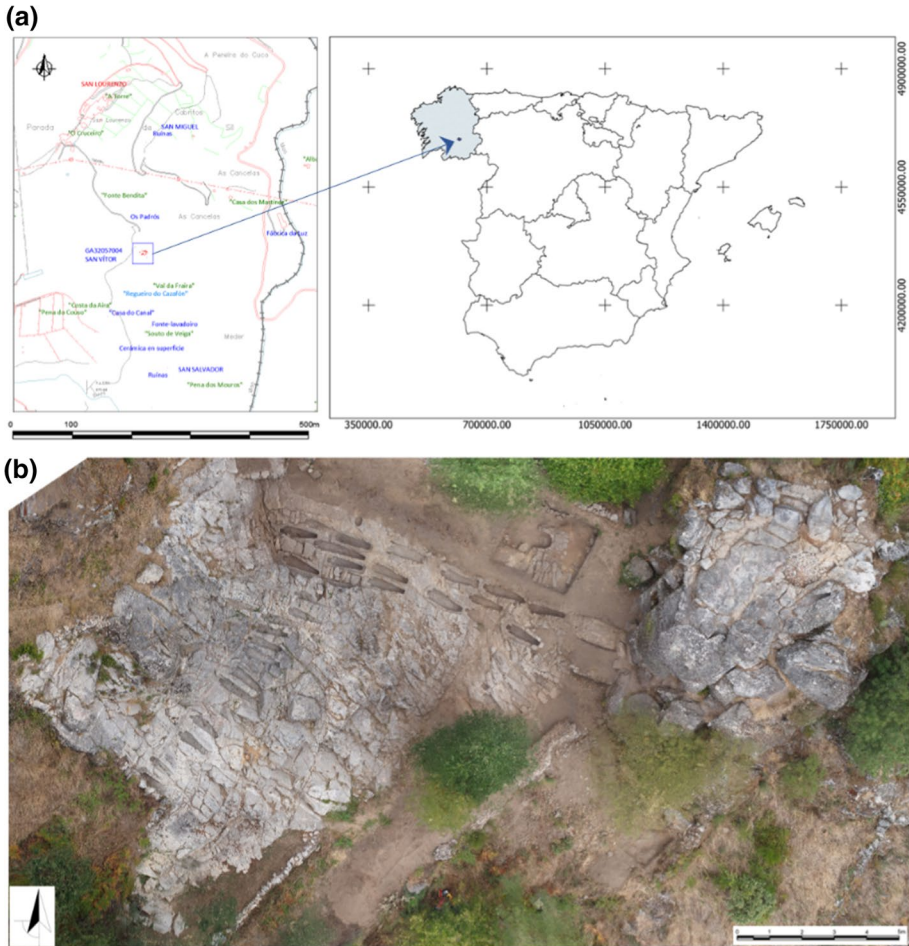
(a)

(b)

Fig. 1 Location of the necropolis of San Vítor de Barxacova in Galicia, NW Spain (**a**), and orthoimage showing a general view of the complex (**b**)

were visible before the archeological intervention, fifty-six anthropomorphic graves dated between the ninth and tenth centuries were finally revealed. Afterward, from 2013 to 2018, successive archeological campaigns were performed for maintenance and restoration.

The site consists of two well-differentiated sectors: A high rock, or Thor, on the east and a granite outcrop or dorsal on the west, in which the necropolis is placed. As seen in Fig. 1b, the graves are east–west oriented and distributed in two different areas, north, and south. In the northern sector, the graves were carved in an orderly manner on a horizontal surface of the outcrop, previously cut and apparently corresponding to construction prior to the necropolis, while in the southern sector the graves were directly carved into the natural rock following a fan pattern distribution.

Regarding the Thor, it contains the remains of the foundations of the San Víctor chapel, with a surface no more than 12 m^2. Around the chapel, there are four anthropomorphic graves, among them the so-called privileged grave which was built with decorative granite stones reused from some previous construction. Moreover, some bone remains appeared in

this grave, dated at the end of the tenth century (obtained by C^{14} analysis), thus informing us of the time maximum use of the chapel and therefore of the necropolis.

In the northern sector, outside the area occupied by the granite outcrop, a semicircular bell smelting furnace, dating between the end of the ninth century and the beginning of the tenth century (obtained by thermoluminescence), was found. This dating gives the moment of culmination of the chapel, or at least of its bell tower, matching with the dating provided by the bone remains in the "privileged grave." Moreover, remains of the foundations of various constructions were found in the necropolis area, some of them prior to the necropolis, and others may be contemporary.

2 Materials and Methods

2.1 Characterization of the Necropolis

Before executing conservation and restoration work on any archeological site, it is necessary to carry out prior diagnoses and analyses. Without these preliminary works, treatment could not meet the minimum guarantee for a successful intervention. They should be therefore considered as inseparable works that complement each other. In situ diagnosis, together with physical, chemical, and biological analyses, contributes to defining the best conservation treatment to control the different degradation processes that interact in archeological sites. Through diagnosis, the different agents, processes, and forms of alteration present in any cultural heritage asset can be precisely characterized.

The necropolis of San Vítor de Barxacova presents an active and entropic thermodynamic environment, in which the alteration processes are mainly due to external factors such as water, temperature, and biological action, as well as other intrinsic properties of the site such as the geology (age of the rock mass—quaternary, type of magma cooling, decompression, etc.) and mineralogical composition of the granite. Thus, various forms of superficial alteration are easily identified by visual inspection, among them, fissures, fractures, loose fragments, holes or disintegration, and sandblasting. Figure 2 shows, for each grave, the alteration forms registered during diagnosis, while Fig. 3 represents the percentage of occurrence obtained for each damage in the archeological complex. The
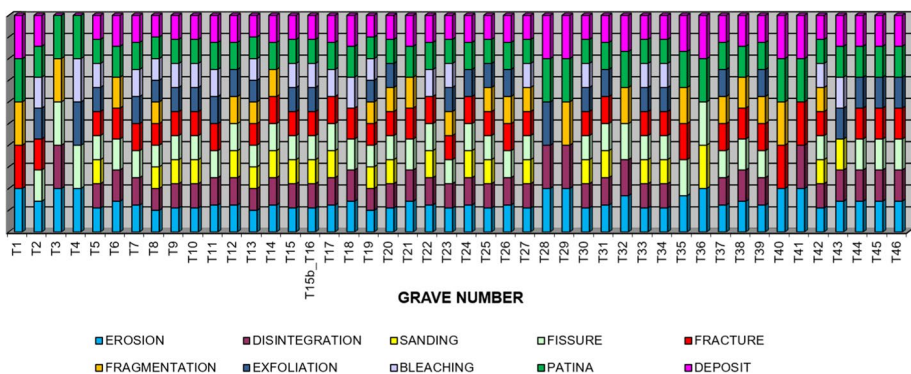

Fig. 2 Forms of superficial alteration recorded for each grave (adapted from Buceta and Carrera 2013)
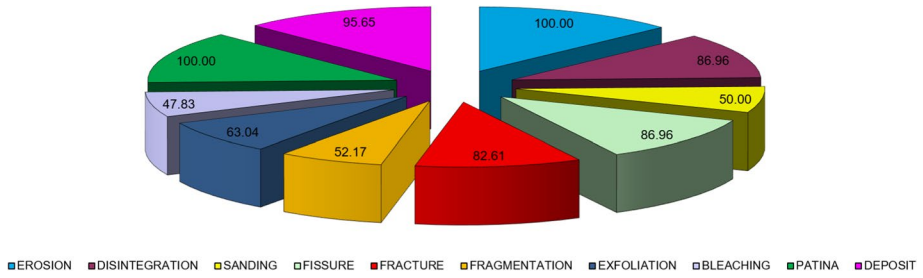
Fig. 3 Percentage of occurrence for each of the damages with respect to the total number of graves (adapted from Buceta and Carrera 2013)

terminology used to describe the alteration forms is based on the ICOMOS glossary (ICO-MOS-ISCS 2008).

Additional studies were carried out to better understand the state of conservation of the granite in the necropolis; thus providing a more detailed diagnosis and prioritizing critical areas or graves at risk. The most relevant analyses performed are:

1. At the macroscopic level. The complex is placed on a granite belonging to the Hercynian period, being a non-oriented two-mica granite with common fine-grained facies (although coarse-grained facies are also presented) and non-oriented porphyry type with mega crystals of quartz, feldspars, and muscovite. Therefore, a granite with varied textures, both equigranular and non-equigranular. The results obtained by simple compressive strength analysis (point load test) revealed an average strength of 54.14 MPa (Zúñiga 2018); whereas the most resistant granite in the complex resulted in a compressive strength higher than 250 MPa. Overall, the complex has relatively low resistance for its type of granite, which resulted in lower in the areas where the graves are placed more certainly due to weathering and degradation. In addition, as illustrated in Fig. 4, fractures can be observed in three main directions. These fractures penetrate deeply and in some cases in opposite directions.

2. At the microscopic level. In a petrographic microscope, the granite showed a non-equigranular texture consisting of feldspar grains with a subdimorphic habit, and signs
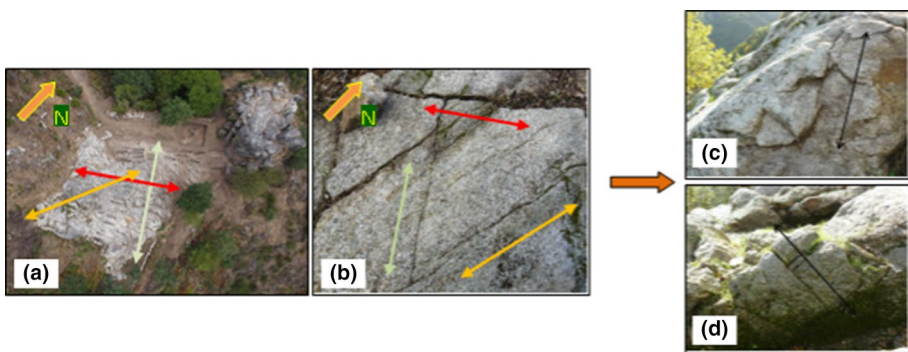

Fig. 4 Main directions of the fractures according to the orientation of the necropolis: macro and detailed view (**a** and **b**, respectively) and fractures in vertical section (**c** and **d**)

of cataclasis with non-uniform extinction and rests of neoformations minerals that prove the degradation of certain constituent minerals (De Rosario et al. 2017). The degradation of biotite to sillimanite, or chlorite and plagioclase to sericite and kaolinite, was therefore confirmed. As shown in Table 1, the low density and high porosity values obtained are typical in exposed granites; thus, indicating severe weathering. Positively, the presence of salts and the electrical conductivity measured in samples were low. The granite, in general, presents interconnected and intraconnected porosity and, therefore, the high values obtained in this case indicate an important expansion of the capillary system. The porosity favors water infiltration into the interior of the rock thus contributing to accelerate the weathering of the constituent minerals, mainly feldspars and micas.

3. Other studies focused on biological agents, which allowed identifying different species of herbaceous plants, lichens, fungi, and algae. It should be noted the low variability of lichen species is due to the microclimatic homogeneity of the site that is exposed and sunny (Sánchez-Biezma 2021). The biological alteration in the complex is slow but continuous, which strongly determines its state of conservation.

Furthermore, it was confirmed that the presence and activity of ants in the inner surface of the graves represent another of the main agents of alteration. In the process of building their anthills, they extract loose grains of weathered material thus contributing to disintegration. Occasionally, it is possible to observe these deposits accumulated on the surface of the graves, with a height of at least 2 cm.

2.2 GPR Applied to Monumental Stone Conservation

In cultural heritage, the GPR method is successfully employed for a great variety of applications, such as locating and mapping buried archeological artifacts, to inspect ancient buildings, bridges, columns, and statues, and investigating frescoes, mosaics, and decorations (Conyers 2004; Goodman and Piro 2013). In the particular case of the GPR application to monumental stone conservation, only a few published works can be found, compared to other applications of the technique such as archeological investigations.

In Giunta and Calloni (2000), GPR was applied to evaluate the condition of conservation of the façade of St. Peter's Basilica in the Vatican. Different antenna frequencies were used (1.5 GHz, 900 MHz, 400 MHz, and 200 MHz) and significant information on the internal structure was obtained (travertine stone, masonry structure, plugs, cramps irons, cavities, detachments, fractures, and cracks). In Binda et al. (2003), a GPR study (500 MHz and 900 MHz antennas) was conducted to investigate the piers and walls of the Cathedral of Noto, which revealed internal inhomogeneities in the masonry and moisture content. In Ranalli et al. (2004), GPR surveys, with 600 MHz and 1.6 GHz antennas, were applied to the structural monitoring of the façade of the Collemaggio Basilica (L'Aquila, central Italy). The results obtained allowed estimating the walls thicknesses, as well as mapping internal structural features and defects (such as detachments, voids, and degraded mortar). In Leucci et al. (2007), a GPR survey conducted with 1 GHz and 1.5 GHz antennas has revealed the existence of fractures in some columns of the crypt of the Cattedrale di Otranto (Apulia, Italy). In Masini et al. (2007) and Nuzzo et al. (2010), GPR investigations are included to evaluate the state of preservation of the thirteenth century rose window of Troia Cathedral (Apulia, Italy). The GPR survey was performed using 1.5 GHz and 900 MHz antennas, providing relevant findings such as fractures, iron bolts, and internal structure of the ashlar curb linking the

Table 1 Physical properties and semiquantitative study of salts and conductivity (adapted from Buceta and Carrera 2013)

	pH (dissolution)	Porosity (%)	Real Density (g/cm^3)	Chlorides (mg/l Cl$^-$)	Sulfates (mg/l SO$_4$$^{2-}$)	Nitrates (mg/l NO$_3$$^-$)	Nitrites (mg/l NO$_2$$^-$)	Conductivity (µS)
Sample1	6.75	12.24	2.79	0	<200	0–10	0–1	1.2
Sample2	6.81	12.00	2.68	0	<200	0	0–1	2.6
SampleMa	6.81	9.80	2.67	0	<200	=0	0–1	1.1

rose window to the façade. In Barone et al. (2010), two different case studies on stone conservation in Rome, Italy, are included: the GPR detection of fractures and internal damages in an ancient Roman Portico "*Porticus Octaviae*" (500 MHz and 1 GHz antennas) and the investigation of the internal structure of the vaulted ceilings of the Zuccari Palace hosting ancient frescoes (900 MHz antenna). In Masini et al. (2010), the GPR method was employed to inspect the columns in the church of San Giovanni al Sepolcro (Brindisi, Italy). A 1.5 GHz antenna was used, and the results produced allowed identifying reinforcement bars, and medieval metallic hinges). In Leucci et al. (2011), a GPR study was performed to determine the deterioration status (cracks and inhomogeneities in inner structure) of the pillars of the Cathedral of Tricarico (southern Italy). In Pérez-Gracia et al. (2013), GPR was employed to define the internal structural configuration of the Cathedral of Saint Mary (Mallorca, Spain). 900 MHz and 1.5 GHz center frequency antennas were used, and the results revealed the internal structure of columns, walls, and buttresses, as well as possible fissures in junctions between ashlars. In Soldovieri et al. (2017), a central frequency of 2 GHz was applied to evaluate the state of conservation of columns (with circular and rectangular sections) in the archeological site of Pompei. The results revealed the presence of reinforcement structures in some of the investigated columns. In Catapano et al. (2018), a 2 MHz GPR study was carried out to map crack patterns and internal cavities in a wall at the Loggia of the Consoli Palace of Gubbio (Italy). In Ortega et al. (2019), a GPR study was performed on the altar wall of the Santa Maria Huiramangaro Church (Michoacán, Mexico). Using 1.5 GHz and 900 MHz antennas, the GPR data provided information about the stone and mud arrangements, and probable small cavities or rock fragments deeply in the wall. In Solla et al. (2021), 500 MHz, 800 MHz, and 2.3 GHz antennas were used to map different stone thicknesses on the façade of the Monastery of Batalha (Leiria, Portugal) aimed to distinguish between the original and recent ashlars.

In Kadioglu et al. (2015), a GPR survey was performed with an 800 MHz antenna through the façade of the "Yazilikaya" Midas Monument (Central Anatolia, Turkey) to detect fractures. In Santos-Assunçao et al. (2016), GPR measurements were made to evaluate the state of conservation of the buried Mycenaean monument Tholos Acharnon tomb (Acharnes, Greece). Using 2.3 GHz and 1.0 GHz antennas, it was possible to define the internal structure of the walls (the stone layers and thicknesses), internal damages such as cracks and voids, and the existence of high salt content in different zones of the structure. In Solla et al. (2014) and (2011), GPR investigations were carried out (using 500 MHz and 250 MHz antennas) to evaluate the internal state of two medieval masonry arch bridges, and the results revealed the existence of hidden arches or a cavity in one pier of the structure, respectively. In Conde et al. (2017), an 800 MHz antenna was used to measure the thicknesses of granitic ashlars in abutments and spandrel walls, paving, and arches of the medieval Vilanova bridge (Galicia, Spain), which allowed to build an accurate and detailed 3D finite element model of the bridge. In Solla et al. (2012), horizontal and vertical accuracies of 8.5% and 2.8%, respectively, were obtained for the thickness estimation of stone blocks from 1 GHz GPR data.

Kadioglu (2013) offers an example of GPR applied to monitor monumental statues of the Anitkabir mausoleum (Ankara, Turkey). Using a 1.6 GHz antenna, it was possible to reveal internal cavities and fractures. In Dimitriadis (2015), five marble statues from the "Antikythera Shipwreck" collection at the National Archeological Museum of Athens (Greece) were investigated using a 2.4 GHz antenna to locate the metal targets used for reassembly during restoration.

2.3 GPR Data Acquisition and Processing

2.3.1 GPR Measurements Setup

GPR data acquisition was conducted with a ProEx system from the company Malå Geoscience, equipped with a ground-coupled antenna having a central frequency of 2.3 GHz (Fig. 5a). This is the highest frequency antenna provided by the company offering the most suitable spatial resolution to define small damages such as fractures or voids. Data acquisitions were carried out using the common-offset mode by distance, and the acquisition parameters were a trace-interval of 1 cm and a total time window of 11 ns (composed of 368 samples per trace by default). The antenna was mounted in a survey cart with an odometer wheel to measure the profile length and to control the trace-interval distance. All the GPR profile lines were carried out at the center of the grave, along the feet-to-head longitudinal direction (Fig. 5b).

Additionally, a three-dimensional (3D) GPR methodology was performed in grave no. XLII (Fig. 5c). A total of 11 parallel 2D profile lines were registered at regular intervals of 2 cm spacing. All the profile lines were collected in the same direction, starting from the lower right corner along the X-axis.

2.3.2 Signal Filtering and Processing

The GPR signals received were processed with the commercial software ReflexW (Sandmeier 2022) by using the processing sequence described in Table 2. The objective was to correct the down-shifting of the radar section due to the air-ground interface (time-zero correction), to remove the initial DC signal component, or DC bias, in the radar traces as the averaged level of the signal is moved from zero amplitude to a different value (dewow), to amplify the received signal to mitigate the energy decay (gain), to remove horizontal continuous low-frequency reflectors (background removal), to remove both low- and high-frequency signal noise in the vertical and horizontal directions (bandpass), and to suppress strong clutter (migration).
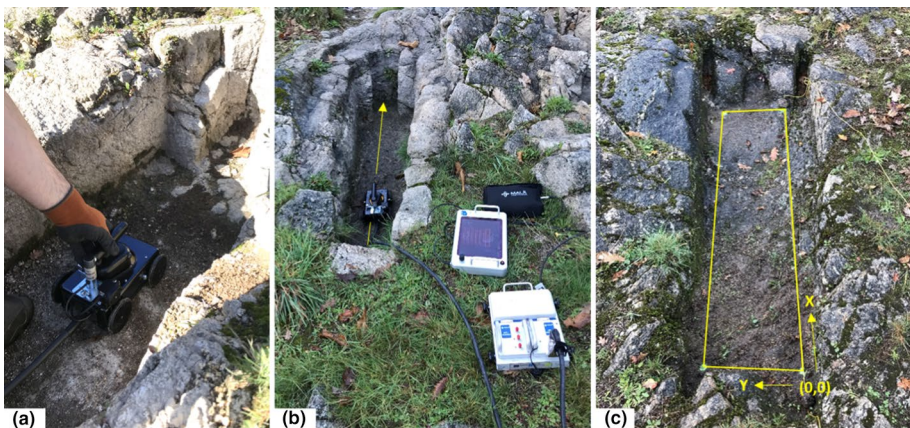
Fig. 5 GPR system used for data acquisition: **a** 2.3 GHz antenna and survey cart, **b** direction of the GPR profile lines, **c** 3D grid in grave no. XLII

Table 2 Filters and settings used for GPR data processing

Filters	Parameters
Time-zero correction	− 1.0 ns
Subtract-mean (dewow)	Time window: 0.5 ns
Gain Function (Linear-Exponential)	Linear: 3 and exponential: 3
Background removal	Default
Bandpass (Butterworth)	Lower: 1200 and upper: 4200 MHz
Migration (Kirchhoff)	Velocity (hyperbola fitting): 0.1 m/ns

The processed data were exported to a MALA RD3 format and then imported into Matlab using an internal load.rd3 file routine.

2.3.3 Amplitude-Based Attribute Analysis

Different amplitude-based approaches were tested aiming to emphasize the information content of the data associated to damage (such as fractures and voids) that could be undetectable from a typical GPR data representation (radargram or B-Scan). With the GPR data processed (processing sequence in Table 2), the following images were computed in Matlab:

- Image A: 2D or conventional radargram (XZ image or B-Scan) where the amplitude of the received signal is shown in grayscale, the trace number is on the X-axis, and the travel time of the signal (in nanoseconds) is on the Z-axis. As an example, Fig. 6-a shows image A obtained for grave nº. XIII showing the interpretation of fractures (red lines) and voids (red ellipses). The Z-axis in time was converted into depths by considering an average propagation velocity of 0.1 m/ns, previously estimated using hyperbola fitting.
- Image B: 2D plot of the normalized amplitude outliers. The radargram matrix is normalized in the $[-1,1]$ interval dividing all the cells by the maximum of the absolute value of the matrix. The outliers in the normalized matrix are later detected using the *isoutlier* function in Matlab by considering three different criteria, and plotted, using a color-scale (right side of the subplot): (1) "mean" criterion: those values that are more than three standard deviations away from the mean are considered as outliers, (2) "median" criterion: those values that are more than three scaled MAD from the mean are considered as outliers [The scaled MAD is defined as $c *$ median(abs(A-median(A))), where $c = -1/(sqrt(2) * erfcinv(3/2))$], and (3) "quartiles" criterion: those values that are more than 1.5 interquartile ranges above the upper quartile or below the lower quartile are considered as outliers (MathWorks, 2022). Figure 6b–d present the results for all the three criteria: mean, median, and quartiles, respectively.

Based on the interpretation of Fig. 6, the expected outputs to understand how granite deterioration could be detectable in GPR imaging are:

- The occurrence of internal fractures (red lines in Fig. 6) can be detectable in the GPR data in terms of (1) higher amplitude values in the damage region because of the larger
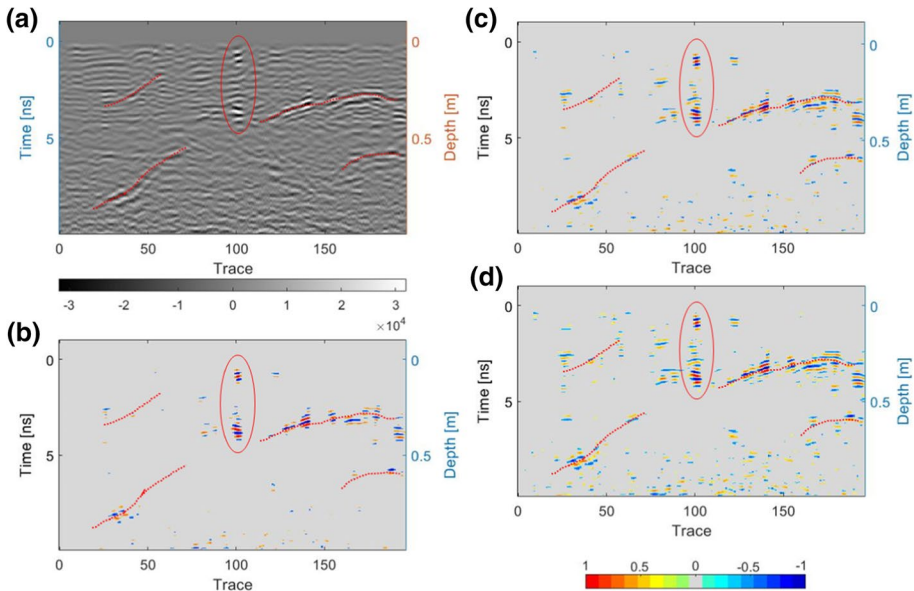
Fig. 6 Example of the amplitude-based imaging generated for grave no. XIII using different configurations: conventional GPR radargram (**a**) and 2D plot of the normalized amplitude outliers with different criterion, mean (**b**), median (**c**) and quartiles (**d**). Imaging also shows the interpretation of internal fractures (red lines) and voids (red ellipses)

dielectric contrast at the interfaces between granite (with a dielectric constant between 5 and 7) and free-space (with a dielectric constant of 1) and (2) continuous reflection patterns reconstructing the fracture shape and orientation distribution.

- The occurrence of voids/cavities (red ellipses in Fig. 6) can be detectable in the GPR data in terms of (1) higher amplitude values in the damage region (as in the case of fractures) and (2) reflection patterns in the form of hyperbolic reflections, in some cases identifying the boundaries of the cavity.

From the interpretation of Fig. 6, it was decided that the best outliers imaging to interpret damages was the median criterion. It is observed how the mean criterion gives less definition in layering fractures, while the quartile criterion showed unwanted outliers (noise).

Moreover, it should be mentioned that the GPR data acquisition was conducted a day after raining for the previous 1–2 h. Superficial cracking and fissures in graves favor water infiltration, thus leading to water accumulation in voids and fracture intersections. In this case study, the presence of water filling damages largely contributes to improving fractures and voids detection. First, the amplitude values become more prominent in the damage region due to the largest dielectric contrast at the interfaces between granite ($K=5-7$) and water ($K=81$) than between granite and air ($K=1$). Second, the phase of the reflected waveforms is reversed (inverse polarity) because the lower medium (water) has a higher dielectric constant than the upper-medium (granite). To illustrate this effect, Fig. 7 shows the GPR data acquired for grave n°. XLIII at two different periods: in October 2021—after raining (a) and in May 2021—after a dry period (b). Interpreting the GPR imaging produced in Fig. 7, it can be observed that the fractures, shape, and orientation, are better
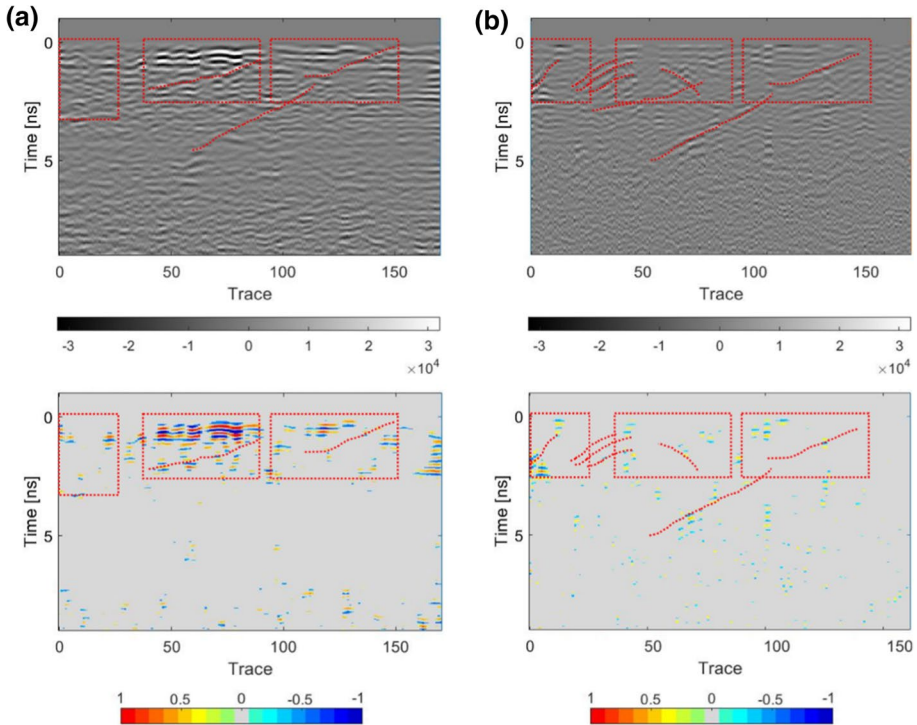
Fig. 7 Comparison of the GPR data acquired for grave no. XLIII at two different periods: **a** after raining and **b** after a dry period. Imaging also shows the interpretation of internal fractures (red lines) and water accumulation (red boxes). Outliers images were obtained with the mean criteria

defined on images under dry conditions, although the received signals have a low amplitude value due to the lower dielectric contrast, and they are not recognized by the outliers method. The images produced under rainy conditions allow identifying critical points of superficial deterioration due to the presence of water infiltration and internal water deposits. The water filling the fracture space produces stronger reflections (high amplitude values) due to the larger dielectric contrast and reduces imaging resolution because of the lower velocity of penetration, thus masking the reflections from the shallow fractures.

Next, for the profile lines collected in the 3D grid performed in grave nº. XLII, the outliers images (Images B) obtained in Matlab were again converted back to the MALA RD3 format and further imported into the 3D data interpretation module of ReflexW to create the 3D cube. This data conversion was made using the save.rd3 file routine available in MATLAB Central File Exchanges (Grinsted 2022).

Finally, the outliers of each profile line were converted to a 3D point representation, and all profile lines collected in the 3D grid were exported to a 3D point cloud to have better visualization in 3D. The lower right corner of the scan grid was considered the reference point of all the scans. Spacing between the points is 1 cm along the X-axis and 2 cm along the Y-axis as the trace-interval was 1 cm during the acquisition, and the grid has 11 parallel 2D profile lines with regular intervals of 2 cm spacing. An average propagation velocity of 0.1 m/ns was used to convert the time to depth in the z-direction. The absolute values of the outliers were assigned to each corresponding point as its scalar value. The dataset can

be exported in common point cloud formats such as LAS and PCD (point cloud library), PLY, and E57. Also, it can be exported to ASCII and ESRI shapefile formats to integrate it within GIS (Geographic Information System) environments.

3 Results and Discussion

A total of 37 graves were surveyed around the necropolis area, although only 13 are shown in this section because of their relevant information or singularity (Fig. 8).

3.1 GPR Main Findings

Table 3 presents the 2D GPR imaging produced with the interpretation of the main findings: (1) the occurrence of superficial fractures or disaggregation (yellow ellipses) due to weathering favors water infiltration; the effect of water throughout time has a negative impact on granite, leading to the formation of internal (2) fractures (red lines) and/or (3) small voids (red ellipses), although, in the worst cases, (4) the water is accumulated in the shallower structure (yellow boxes) contributing to accelerate deterioration. It should be mentioned that the graves are inclined to the southeast (SE), so the water tends to accumulate at their feet, generally being the most deteriorated zone (e.g., graves no. VIII, IX, XIII, XXX, XXXVII, XLII, and XLVIII). In most cases, the GPR results allow for defining sub-vertical fractures parallel distributed (e.g., graves no. VIII, IX, and XV). This later can
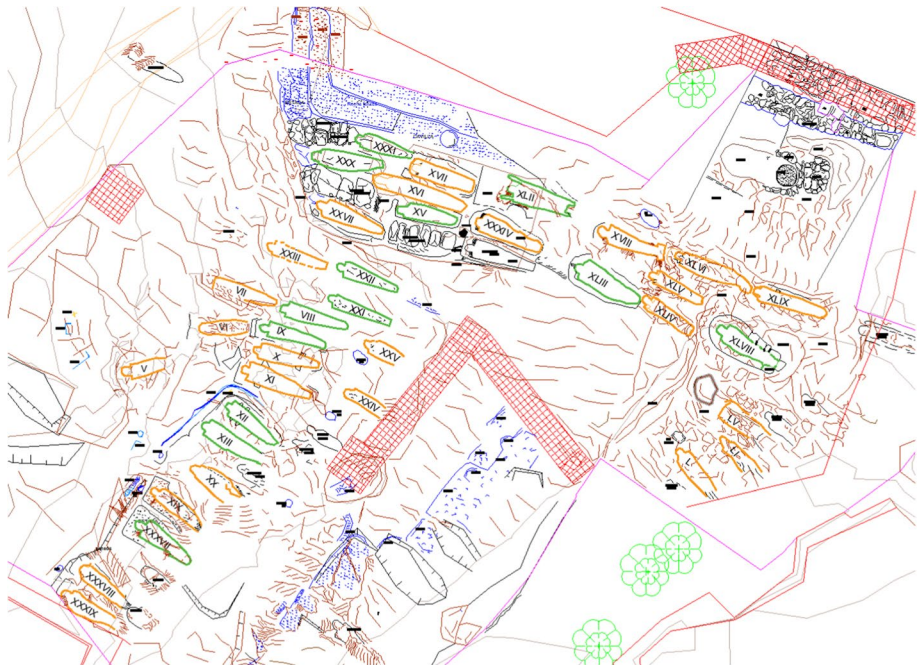
Fig. 8 General overview of the necropolis complex showing the surveyed graves in orange and green colors, being the graves highlighted in green color those selected for discussion in this section

Table 3 2D GPR imaging showing the interpretation of the main findings: superficial fractures or disaggregation (yellow ellipses), internal fractures (red lines), voids (red ellipses), and water accumulation (yellow boxes)
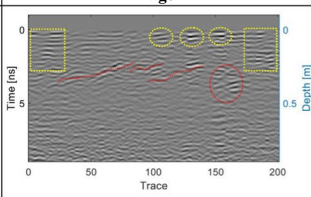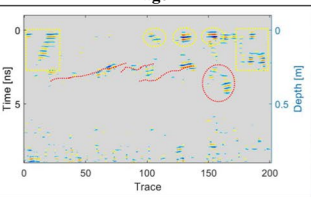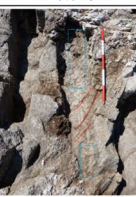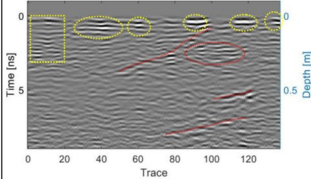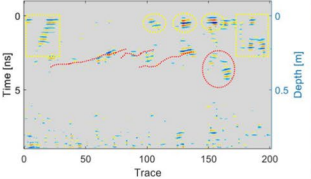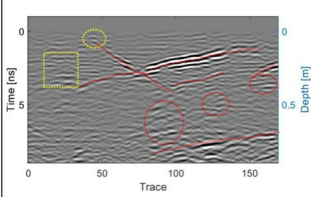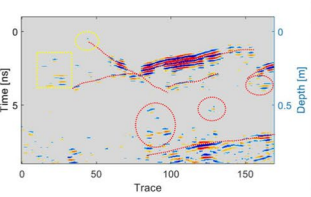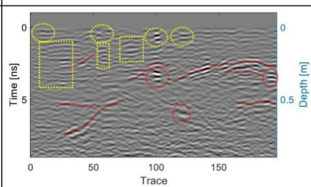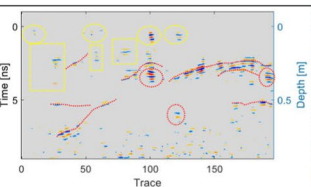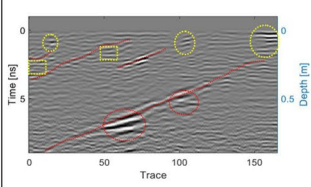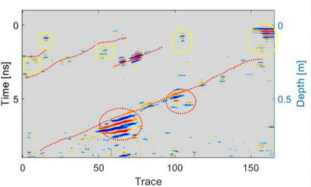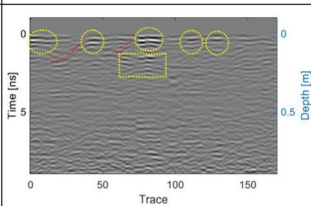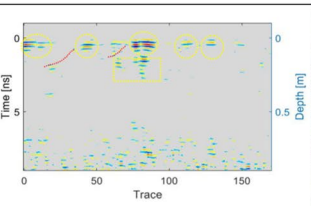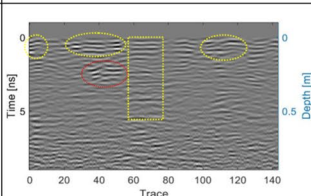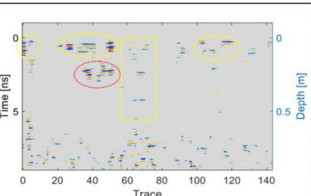
Grave nº.	Image A	Image B	Picture
VIII			
IX			
XII			
XIII			
XV			
XXI			
XXII			

Table 3 (continued)

be beneficial because they support drainage (e.g., grave no. XXX). In graves no. XII and XLVIII, it is possible to observe two different grain directions.

Figure 9 shows the 3D results obtained for grave no. XLII. Observing all the images produced, it was possible to identify water accumulation at the beginning of the GPR profile line (from 0.0 to 0.4 m) and a sub-vertical fracture that extends from 0.7 m to the end of the grave. Moreover, the 3D cube (Fig. 9d) illustrates the XY, YZ, and XZ images for
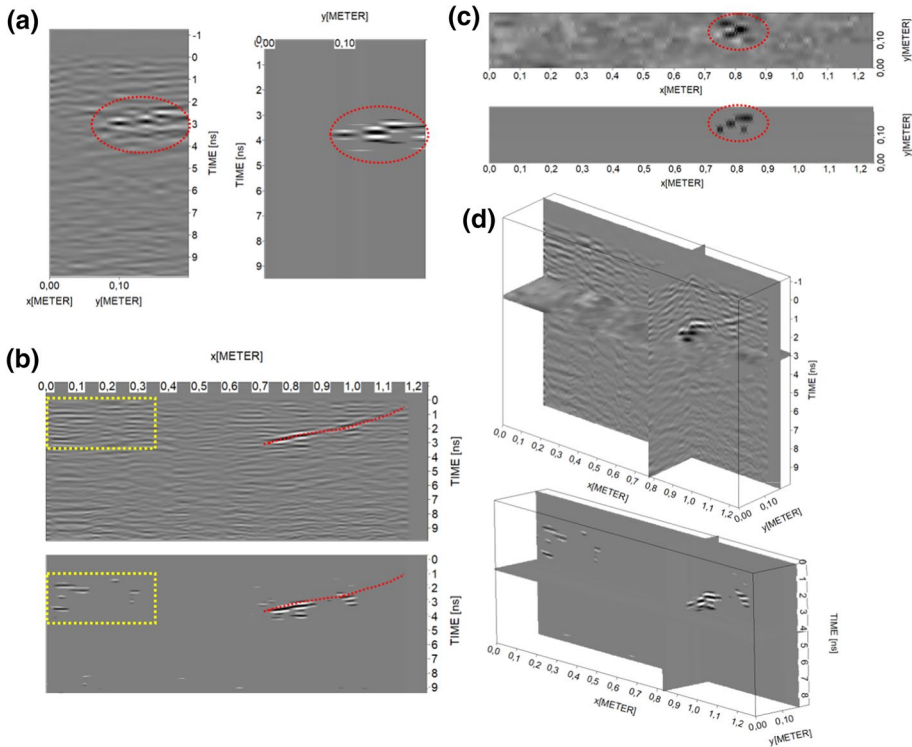
Fig. 9. 3D imaging for grave no. XLII (both the conventional GPR data and the outliers images): **a** YZ image (D-Scan), **b** XZ image (B-Scan), **c** XY image (C-Scan or time-slice) at 15–20 cm depth, **d** schematic representation of the 3D cube showing the propagation of the fracture in perpendicular directions

this damaged area, which allows visualizing the propagation of the fracture, thus providing additional information about damage volume. It is important to mention here that the outliers images used to create the 3D cube are based on the mean criteria to filter the unwanted points (colored pixels) generated from the data conversion.

Finally, Fig. 10 shows different perspectives of the exported point cloud. The amplitude values of the outliers were normalized and colored to enhance the visualization for interpreting damage distribution. For example, the water accumulates heavily in the right corner at the foot of the grave.

3.2 Evaluation of Visualization Strategies Supporting Damage Identification

The outliers imaging proposed in this paper has demonstrated its capabilities to enhance relevant information dealing with graves deterioration (existence of fractures, voids, and water-accumulating deposits). If compared with the conventional GPR images (or radargrams), the outliers images highlight the existence of "anomalies or discontinuities" in a relatively homogenous medium (presence of air or water) which makes easier the interpretation by any non-expert user of the method. Nevertheless, a conventional image provides an overall image of the entire subsurface space and, therefore, it cannot be ignored in the interpretation process because some isolated reflector of interest could be omitted by
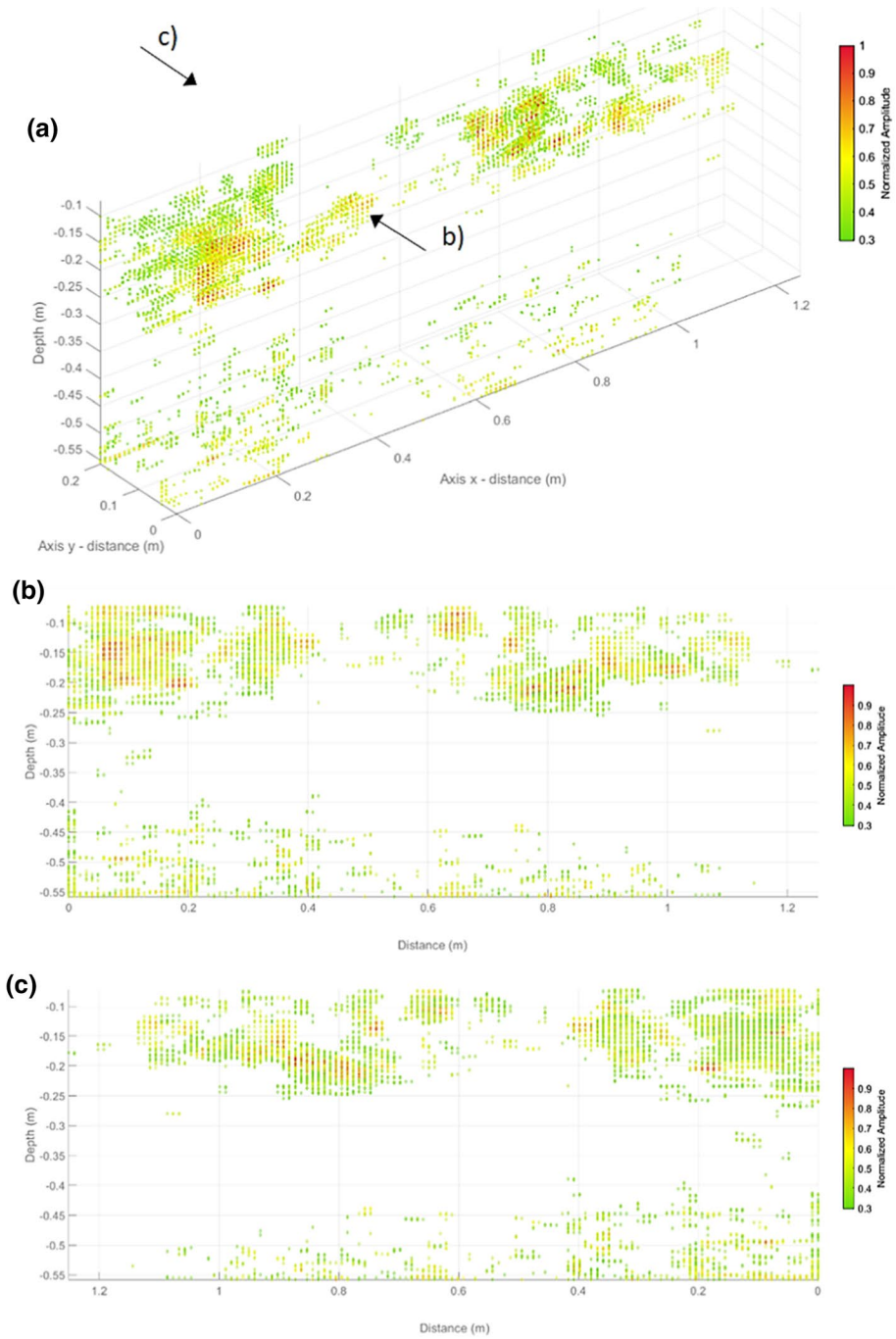
Fig. 10 Exported point cloud of the outliers with their corresponding normalized amplitude values for grave no. XLIII: **a** 3D perspective, **b** and **c** side views of the *X–Z* plane (Visualization in Matlab)

the outliers function (for example the superficial cracks/fractures in graves nº. XII, XIII, XXXVII).

Regarding the different criteria (median, mean, and quartiles) tested for the outliers detection, the median criterion provides the best results from an interpretational point of view, showing a better definition of the damages (e.g., fracture shape). The method based on the quartiles criterion gives a noisier image, while when the mean criterion is used, the relevant reflections are over-filtered. The median criterion was therefore selected for the 2D outliers images. However, for the elaboration of the outliers 3D cube and the imaging of the fracture propagation, the mean criterion was preferred for exhaustive discrimination of the reflections, which allowed for accurate extraction of the damage pattern detected.

The outliers 3D cube and imaging produced for the grave nº. XLII gave more accurate information about damage extent and shape, mainly the volume of water deposits and distribution of the fracture system. Furthermore, the point cloud generated and exported to interoperable GIS formats, if georeferenced, opens the possibility to merge the GPR point cloud of damages detected into a LiDAR point cloud of the necropolis complex. Advanced spatial analysis and simulations can be then performed aiming to correlate different terrain aspects and climatic variables (e.g., slope map, orientation map, etc.) with the damages detected by GPR, which also improve the understanding of the granite alteration mechanisms at the site.

4 Conclusions

This work presents the particular case study of the necropolis of San Vítor de Barxacova in NW Spain. Through the use of different amplitude-based imaging and visualization strategies, it was shown how the GPR method provided a valuable contribution toward the assessment of anthropomorphic graves carved into a natural granite rock. In particular, the GPR tests using a high-frequency 2.3 GHz antenna were conducted to locate and map internal damages such as fractures or deposits of water accumulation. It was demonstrated how the outliers detection gave a better definition than conventional GPR images to highlight the existence and definition of such subsurface defects. Moreover, the 3D visualization of the outliers cube generated allows for a more suitable understanding of the extent, shape, and orientation distribution of the detected defects. Finally, digitizing the extracted information into a point cloud format opens new possibilities for 3D visualization with the surrounding environment, better integration with GIS (Geographic Information Systems), and advanced modeling for complete scene reconstruction.

To conclude, the imaging and visualization approach developed in this paper allows for a better knowledge of the state of conservation of the granitic rock where the graves are located and permits an evaluation of their health status. Thus this provides data that are crucial to support decision-makers engaged in conservation and restoration work: (1) to know areas with voids where to perform a consolidation (using inorganic materials) in order to strengthen the resistance of the rock; (2) to know and understand the fracture distribution to better plan where the consolidating material can easily penetrate; (3) to evaluate the depth of penetration of the consolidating material through the fracture system; and (4) to decide where to place bonding bolts to join fractured rocks.

References

Annan P (2003) GPR principles, procedures and applications. Sensors and Software Inc., Mississauga, p 278

Barone PM, Di Matteo A, Graziano F, Mattei E, Pettinelli E (2010) GPR application to the structural control of historical buildings: two case studies in Rome, Italy. Near Surf Geophys 8:407–413

Binda L, Saisi A, Tiraboschi C, Valle S, Colla C, Forde M (2003) Application of sonic and radar tests on the piers and walls of the Cathedral of Noto. Constr Build Mater 17:613–627

Buceta G, Carrera F (2013) Memorias: porpostas de conservación-restauración das tumbas da necrópole de San Vítor de Barxacova (Parada de Sil, Ourense) [in Galician]. Dirección Xeral de Patrimonio Cultural, Xunta de Galicia

Catapano I, Ludeno G, Soldovieri F, Tosti F, Padeletti G (2018) Structural assessment via ground penetrating radar at the consoli Palace of Gubbio (Italy). Remote Sens 10:45

Conde B, Ramos LF, Oliveira DV, Riveiro B, Solla M (2017) Structural assessment of masonry arch bridges by combination of non-destructive testing techniques and three-dimensional numerical modelling: Application to Vilanova bridge. Eng Struct 148:621–638

Conyers LB (2004) Ground-penetrating radar for archaeology. Geophysical methods for archaeology. Altamira Press, Lanham

De Rosario I, Rivas T, Buceta G, Feijoo J, Mosquera MJ (2017) Surfactant-synthesized consolidants applied to a granite medieval necropolis in NW Spain. Laboratory and in situ effectiveness evaluation. Int J Archit Heritage 11(8):1166–1176

Dimitriadis K (2015) GPR in the preservation of cultural heritage. In: Proceedings of third general meeting, COST action TU1208, London, UK, March. Aracne, Ariccia. Book series: COST Action TU1208, Rome, Italy

Giunta G, Calloni G (2020) Ground penetrating radar applications on the façade of St. Peter's Basilica in Vatican. In: 15th WNDT, Rome

Goodman D, Piro S (2013) GPR remote sensing in archaeology, geotechnologies and the environment, vol 9. Springer, Berlin

Grasmueck M, Weger R, Horstmeyer H (2005) Full-resolution 3D GPR imaging. Geophysics 70(1):K12–K19

Grinsted A (2022) RD3 Library. MATLAB central file exchange. https://www.mathworks.com/matlabcentral/fileexchange/6129-rd3-library. Retrieved Jan 27, 2022

ICOMOS-ISCS (2008) Illustrated glossary on stone deterioration patterns. Monuments and sites XV, Ateliers 30 Impression, Champigny/Marne, France

Kadioglu S (2013) Tansparent 2d/3d half bird's-eye view of ground penetrating radar data set in archaeology and cultural heritage. Chapter 5 in: Imaging and radioanalytical techniques in interdisciplinary research—fundamentals and cutting edge applications

Kadioglu S, Kadioglu KY, Akyol AA (2015) Picturing monuments and cultural heri-tages with ground penetrating radar method including its half bird' s eye view visualiza-tion. In: Proceedings of the 8th international workshop on advanced ground penetrating radar (IWAGPR), 7–10 July, Florence, Italy: 1–4

Leucci G, Cataldo R, De Nunzio G (2007) Assessment of fractures in some columns inside the crypt of the Cattedrale di Otranto using integrated geophysical methods. J Archaeol Sci 34(2):222–232

Leucci G, Masini N, Persico R, Soldovieri F (2011) GPR and Sonic tomography for structural restoration: the case of the cathedral of Tricarico. J Geophys Eng 8(3):76–92

Masini N, Nuzzo L, Rizzo E (2007) GPR investigations for the study and restoration of the rose window of Troia Cathedral (southern Italy). Near Surf Geophys 5(5):287–300

Masini N, Persico R, Rizzo E, Calia A, Giannotta MT, Quarta G, Pagliuca A (2010) Integrated techniques for analysis and monitoring of historical monuments: the case of San Giovanni al Sepolcro in Brindisi (Southern Italy). Near Surf Geophys 8(5):423–432

MathWorks (2022) Find outliers in data—MATLAB isoutlier. https://es.mathworks.com/help/matlab/ref/isoutlier.html. Retrieved Feb 21, 2022

Nuzzo L, Calia A, Liberatore D, Masini N, Rizzo E (2010) Integration of ground-penetrating radar, ultrasonic tests and infrared thermography for the analysis of a precious medieval rose window. Adv Geosci 24:69–82

Ortega-Ramírez J, Bano M, Larrea-López L, Robles-Camacho J, Ávila-Luna P, Villa- Alvarado LA (2019) GPR measurements to identify cracks and textural arrangements in the altar wall of the 16th century Santa Maria Huiramangaro Church, Michoacán, Mexico. Near Surf Geophys 17(3):247–261

Pérez-Gracia V, Caselles JO, Clapés J, Martinez G, Osorio R (2013) Non-destructive analysis in cultural heritage buildings: evaluating the Mallorca cathedral supporting structures. Non Destruct Test Evaluat Int 59:40–47

Ranalli D, Scozzafava M, Tallini M (2004) Ground penetrating radar investigations for the restoration of historic buildings: the case study of the Collemaggio Basilica (L'Aquila, Italy). J Cult Herit 5:91–99

Sánchez-Biezma MJ (2021) Estudos transversais na necrópole rupestre de San Vitor de Barxacova GA32057004 [*in Galician*]. Dirección Xeral de Patrimonio Cultural, Xunta de Galicia

Sandmeier K (2022) ReflexW. Manual version http://www.sandmeier-geo.de. Accessed Jan 2022

Santos-Assunçao S, Dimitriadis K, Konstantakis Y, Perez-Gracia V, Anagnostopoulou E, Gonzalez-Drigo R (2016) Ground-penetrating radar evaluation of the ancient Mycenaean monument Tholos Acharnon tomb. Near Surf Geophys 14(2):197–205

Soldovieri F, Masini N, Persico R, Catapano I (2017) GPR diagnostics of columns in archaeological contexts. In: Geophysical Research Abstracts, vol 19, EGU General Assembly

Solla M, Lorenzo H, Riveiro B, Rial FI (2011) Non-destructive methodologies in the assessment of the masonry arch bridge of Traba, Spain. Eng Fail Anal 18:828–835

Solla M, González-Jorge H, Álvarez MX, Arias P (2012) Application of non-destructive geomatic techniques and FDTD modeling to metrical analysis of stone blocks in a masonry wall. Constr Build Mater 36:14–19

Solla M, Riveiro B, Lorenzo H, Armesto J (2014) Ancient stone bridge surveying by ground-penetrating radar and numerical modeling methods. J Bridg Eng 19(1):110–119

Solla M, Gonçalves LMS, Gonçalves G, Francisco C, Puente I, Providência P, Gaspar F, Rodrigues H (2021) A building information modeling approach to integrate geomatic data for the documentation and preservation of cultural heritage. Remote Sens 12:4028

Zuñiga D (2018) Caracterización geotécnica del macizo de la necrópolis de San Vítor de Barxacova. Implicaciones en su conservación [*in Spanish*]. Universidade de Vigo

Authors and Affiliations

Mercedes Solla[1] · Gonzalo Buceta-Bruneti[2] · Ahmed Elseicy[1] · Breogán Nieto-Muñiz[3]

Gonzalo Buceta-Bruneti
gonzalo.buceta@gmail.com

Ahmed Elseicy
ahmedmossadibrahim.elseicy@uvigo.es

Breogán Nieto-Muñiz
info@breoganarqueoloxia.com

[1]   CINTECX, GeoTECH Research Group, Universidade de Vigo, 36310 Vigo, Spain

[2]   Curator and Restorer of Cultural Heritage, 36005 Pontevedra, Spain

[3]   Professional Archaeologist, 32004 Ourense, Spain